NASA Technical Memorandum 79030

MODAL PROPAGATION ANGLES IN A CYLINDRICAL DUCT WITH FLOW AND THEIR RELATION TO SOUND RADIATION

Edward J. Rice and Marcus F. Heidmann
Lewis Research Center
Cleveland, Ohio

and

Thomas G. Sofrin
Pratt and Whitney Aircraft
East Hartford, Connecticut

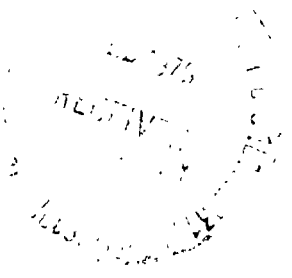

TECHNICAL PAPER to be presented at the
Seventeenth Aerospace Sciences Meeting
sponsored by the American Institute of
Aeronautics and Astronautics
New Orleans, Louisiana, January 15-17, 1979

MODAL PROPAGATION ANGLES IN A CYLINDRICAL DUCT WITH FLOW AND THEIR RELATION TO SOUND RADIATION

Edward J. Rice* and Marcus F. Heidmann**
National Aeronautics and Space Administration
Lewis Research Center
Cleveland, Ohio 44135

and

Thomas G. Sofrin†
Pratt and Whitney Aircraft
East Hartford, Connecticut 06108

Abstract

The angles of propagation of the wave fronts associated with the duct modes are derived for a cylindrical duct with a uniform steady flow. These are the angles which the normal of the local wave front makes with the coordinate axes. The main emphasis is upon the propagation angle with respect to the duct axis and its relation to the far-field acoustic radiation pattern. When the steady flow Mach number is accounted for in the duct, the propagation angle in the duct is shown to be coincident with the angle of the principal lobe of far-field radiation obtained using the Wiener-Hopf technique. Different Mach numbers are allowed within the duct and in the external field. Some interesting results of the analysis have implications regarding static noise tests and external flow convective effects. For static tests with a steady flow in an inlet but with no external Mach number the far-field radiation pattern is shifted considerably toward the inlet axis when compared to zero Mach number radiation theory. As the external Mach number is increased the noise radiation pattern is shifted away from the inlet axis. The theory is developed using approximations for sound propagation in circular ducts. An exact analysis using Hankel function solutions for the zero Mach number case is given to provide a check of the simpler approximate theory.

E-9826

Introduction

The angle which the wave front normal vector makes with the duct axis is significant since this angle governs the location of the principal lobe of the far-field radiation. This has been shown in semi-infinite rectangular ducts with uniform flow by Wright[1] and Cerdel[2] and in circular ducts for the no-flow case by Homicz and Lordi.[3] Steady flow in the duct will be shown to have an important effect upon the far-field radiation pattern.

Also of significance is the angle which the wave front normal makes with the radial coordinate which is the angle of incidence upon the wall. This angle of incidence is intimately related to the mode cut-off ratio which has been shown by Rice[4,5] to correlate the performance of acoustic suppressors. The angle of incidence upon the wall is also necessary for ray tracing techniques as used by Posey[6] Ray tracing techniques were also used by Jacques[7] to obtain approximate flight effects upon sound radiating from jet exhaust pipes. In refs. 6 and 7 the connection between the acoustic ray angles and the duct modes were not considered. It should be noted when considering angles of propagation of the wave fronts comprising a mode in a soft-wall duct, that these angles will be modified by the acoustic liner boundary condition. This effect will be reported in a separate paper.[8]

The angles of propagation will be derived from the convective wave equation and its solutions. Additional convective effects must then be considered both in the duct and in the far-field so that inferences can be made regarding the far-field radiation for both static and external flow conditions. These cases are handled by allowing different Mach numbers in the duct and in the surrounding medium. Approximations will be used to obtain simplified equations for the angles of propagation. Exact solutions for these angles using Hankel function solutions are given in appendix A and are used to check the approximations made in the main text.

Symbols

$C_{m\mu}$	modal pressure coefficient, see eqs. (2), (A-2) and (A-3), N/m^2
c	speed of sound, or the magnitude of the wave velocity vector normal to a plane wave front, m/sec
c_i	components of vector c, i = x, r, θ, m/sec
c_R	resultant velocity vector, m/sec
$H_m^{(1)}$	Hankel function of first kind and order m, see eq. (A-4)
$H_m^{(2)}$	Hankel function of second kind and order m, see eq. (A-4)
h_m	magnitude of $H_m^{(1)}$
J_m	Bessel function of the first kind of order m
K	magnitude of $\vec{K}$, m^{-1}
K'	dimensionless local wavenumber, see eq. (A-18)
$\vec{K}$	local wave number vector, m^{-1}
k	wave number, ω/c, m^{-1}
k_r	radial wave number, m^{-1}
$k_{r\theta}$	combined radial-circumferential wave number (α/r_o), m^{-1}
k_x	axial wave number, m^{-1}
k_y	transverse wave number in rectangular duct, m^{-1}
k_θ	circumferential wave number, m^{-1}
M	Mach number
M_D	Mach number in duct
M_∞	Mach number in surrounding medium
m	spinning mode lobe number
P	acoustic pressure, N/m^2
P_o	far-field pressure for static tests, N/m^2

*Head-Acoustics Section, Member AIAA
**Aerospace Engineer, Member AIAA
†Acoustics Consultant

P_∞ far-field pressure with external flow, N/m^2

P_m^1 outward traveling pressure wave in a cylindrical duct, see eq. (A-2), N/m^2

P_m^2 inward traveling pressure wave in a cylindrical duct, see eq. (A-3), N/m^2

r radial coordinate, m

r_o duct radius, m

S circumferential arc length, m

t time, sec

V_{gx} axial group velocity, m/sec

V_{ph} phase velocity normal to wave front in cylindrical duct, m/sec

x axial coordinate, m

Y_m Bessel function of the second kind and order m

y rectangular coordinate, m

α hardwall duct mode eigenvalue

θ circumferential coordinate, radians

ξ mode cut-off ratio, see eq. (11)

Φ_m phase of $H_m^{(1)}$, radians

φ_r wave front propagation angle relative to radial coordinate, angle of incidence on the wall, deg

φ_s wave front propagation angle with respect to circumferential arc direction, same as φ_θ, deg

φ_x wave front propagation angle relative to axial coordinate, deg

φ_y wave front propagation angle measured from y coordinate, deg

φ_θ wave front propagation angle relative to circumferential coordinate, deg

χ constant phase value, see eq. (A-10), radians

ψ resultant axial propagation angle in duct, deg

ψ_p angle between duct axis and peak of the principal lobe of radiation in the far-field, deg

ω circular frequency, radians/sec

Subscripts

$m\mu$ designates quantity for m^{th} circumferential and μ^{th} radial mode

Development of the Propagation Angles

The wave equation in a circular duct with a steady flow can be expressed as,

$$(1 - M_D^2)\frac{\partial^2 P}{\partial x^2} - 2\frac{M_D}{c}\frac{\partial^2 P}{\partial x \partial t} + \frac{\partial^2 P}{\partial r^2} + \frac{1}{r}\frac{\partial P}{\partial r} + \frac{1}{r^2}\frac{\partial^2 P}{\partial \theta^2} = \frac{1}{c^2}\frac{\partial^2 P}{\partial t^2} \qquad (1)$$

where x, r, and θ are the usual cylindrical coordinates, t is time, M_D is Mach number, c the speed of sound, and P is the acoustic pressure. The solution to eq. (1) for the pressure is,

$$P_{m\mu} = C_{m\mu} J_m\left(\frac{\alpha_{m\mu} r}{r_o}\right) e^{i(\omega t - k_{x,m\mu} x - m\theta)} \qquad (2)$$

where m is the number of lobes for the spinning mode (circumferential order), μ the radial order number of the mode, $k_{x,m\mu}$ is the axial wave number, ω is the circular frequency, r_o is the outer wall radius, $\alpha_{m\mu}$ is the mode eigenvalue, and J_m is the Bessel function of the first kind and order m.

For brevity, the $m\mu$ subscripts will be deleted, and it will be understood that a single (but quite general) mode is being considered. When eq. (2) is inserted into eq. (1) the result is,

$$\left(\frac{\alpha}{r_o}\right)^2 + k_x^2 = k^2 - 2M_D k k_x + M_D^2 k_x^2 = (k - M_D k_x)^2 \qquad (3)$$

The first term in eq. (3) is a combined radial-transverse wave number often denoted by,

$$\frac{\alpha}{r_o} = k_{r\theta} \qquad (4)$$

This combination of wave numbers is, as will be shown later, the cause of the trouble in defining some of the propagation angles in cylindrical ducts.

The approximation will now be made that the wave fronts behave locally as plane waves propagating skewed to the coordinate angles of the duct. The final approximate equations will be checked by an exact but more cumbersome solution using Hankel functions in appendix A. The approximate solutions are found to be sufficiently accurate near the cylindrical duct wall where the angle of incidence would be used and where most of the acoustic intensity usually exists. The i^{th} propagation angle can be defined by,

$$\cos \varphi_i = \frac{k_i}{\sqrt{\sum_i k_i^2}} \qquad (5)$$

which is derived in appendix B, and where i = r, θ, or x and φ_i is the angle between the normal to the wave front and the i^{th} coordinate axis. When there is no flow, eqs. (3) and (4) can be shown to yield the usual result,

$$\sqrt{\sum_i k_i^2} = k, \text{ for } M_D = 0 \qquad (6)$$

and then eq. (5) becomes the standard direction cosine expression,

$$\cos \varphi_i = \frac{k_i}{k}, \text{ for } M_D = 0 \qquad (7)$$

For finite Mach number however, from eqs. (3) and (4),

$$\sqrt{\sum_i k_i^2} = k\left(1 - M_D \frac{k_x}{k}\right) \qquad (8)$$

Axial Propagation Angle

The angle of propagation with respect to the x-axis can be found without further approximation.

The axial wave number can be found by rearranging eq. (3) to yield

$$k_x = \frac{k}{(1 - M_D^2)} \left[-M_D + \sqrt{1 - (1 - M_D^2)\left(\frac{\alpha}{kr_o}\right)^2} \right] \quad (9)$$

where the plus sign has been selected for the radical to provide the expression for the wave traveling in the positive x direction. Eqs. (5), (8) and (9) then yield,

$$\cos \varphi_x = \frac{k_x}{k\left(1 - M_D \frac{k_x}{k}\right)} = \frac{-M_D + \sqrt{1 - (1 - M_D^2)\left(\frac{\alpha}{kr_o}\right)^2}}{1 - M_D \sqrt{1 - (1 - M_D^2)\left(\frac{\alpha}{kr_o}\right)^2}} \quad (10)$$

where all of the quantities in eq. (10) are known. It is convenient here to introduce the mode cut-off ratio,

$$\xi = \frac{kr_o}{\alpha \sqrt{1 - M_D^2}} \quad (11)$$

which is consistent with the derivation of Sofrin and McCann,[9] but where cut-off occurs when $\xi = 1$. Eq. (10) then becomes,

$$\cos \varphi_x = \frac{-M_D + \sqrt{1 - 1/\xi^2}}{1 - M_D \sqrt{1 - 1/\xi^2}} \quad (12)$$

Note that when $M_D = 0$

$$\cos \varphi_x = \sqrt{1 - 1/\xi^2} \quad (13)$$

or

$$\sin \varphi_x = 1/\xi, \text{ for } M_D = 0 \quad (14)$$

which is the same relationship as given for the angle of the peak of the principal lobe of far field radiation as given in refs. 4 and 10. This correspondence between propagation angle with respect to the duct axis and far-field radiation has been noted previously for zero Mach number in refs. 1 to 3. This correspondence will be shown, in the next section, to hold for cylindrical ducts with the same flow in the duct and in the surrounding medium.

Radial and Circumferential Propagation Angles

As noted earlier, eq. (12) can be obtained without additional approximations. However, the angle of incidence on the wall (φ_r) and the angle to the transverse or circumferential direction (φ_θ) cannot be obtained exactly using the present method because as shown in eqs. (3) and (4), the radial and transverse wave numbers are combined through the mode eigen value (α). The transverse wave number can be obtained from eq. (2) as follows,

$$m\theta = k_\theta r\theta \quad (15)$$

where

$$k_\theta = \frac{m}{r} \quad (16)$$

It is reasonable to assume that

$$k_{r\theta}^2 \approx k_r^2 + k_\theta^2 \quad (17)$$

which is the result that would be obtained using a rectangular approximation to a thin annulus and is equivalent to the approach suggested by Cumpsty.[11] Thus using eqs. (4), (16) and (17).

$$k_r \approx \sqrt{\left(\frac{\alpha}{r_o}\right)^2 - \left(\frac{m}{r}\right)^2} \quad (18)$$

and then using eqs. (5) and (8) the other propagation angles can be calculated as

$$\cos \varphi_r \approx \frac{\sqrt{\left(\frac{\alpha}{r_o}\right)^2 - \left(\frac{m}{r}\right)^2}}{k\left(1 - M_D \frac{k_x}{k}\right)} \quad (19)$$

and

$$\cos \varphi_\theta \approx \frac{m}{kr\left(1 - M_D \frac{k_x}{k}\right)} \quad (20)$$

Notice that φ_r and φ_θ vary with duct radius while φ_x does not. Introducing the mode cut-off ratio (eq. (11)) and letting $r = r_o$, the angle of incidence at the wall can be written as,

$$\cos \varphi_r\Big)_{r=r_o} \approx \frac{\sqrt{1 - M_D^2}\sqrt{1 - \left(\frac{m}{\alpha}\right)^2}}{\xi\left[1 - M_D\sqrt{1 - \frac{1}{\xi^2}}\right]} \quad (21)$$

It is now easy to see why the cut-off ratio approximately correlated the optimum wall impedance values for acoustic liners in ref. 4. For a given Mach number and for small m/α the angle of incidence upon the wall is a function only of cut-off ratio. The scatter in the above mentioned correlation occurred mainly for the high circumferential lobe number, low radial order modes where m/α was not small. Eq. (21) shows this ratio to be an additional variable when it is not small. Perhaps a better correlating parameter for optimum impedance would be the angle of incidence upon the wall rather than the cut-off ratio. This has been investigated and will be reported in ref. 8. It should be noted that the soft wall boundary condition will alter the angle of incidence from that given in eq. (21).

Far-Field Radiation Considerations

As mentioned previously the axial angle of propagation has been shown to correspond to the angle of maximum noise propagation in the far-field for zero Mach number. However, for the case of uniform Mach number both in the duct and in the surrounding medium, an expression can be written

from the results of refs. 2, 3, and 12 as,

$$\cos \Psi_p = \sqrt{1 - M^2} \left\{ \frac{1 - \frac{1}{\xi^2}}{1 - M^2\left(1 - \frac{1}{\xi^2}\right)} \right\}^{1/2} \qquad (22)$$

where Ψ_p is the approximate angle for the peak of the principal lobe of radiation in the far field. The zero Mach number case of eq. (22) has been shown to be a close approximation for the location of the peak of the principal lobe of the far-field radiation pattern for unflanged ducts in ref. 3. Saule [13] has shown that using the duct eigenvalue to obtain estimates of the principal lobe peak angle can result in a small error for the case of a flanged duct radiation pattern and he provides a method for applying a correction to this angle if it is considered necessary.

The first objective here is to show that the resultant axial angle of propagation in the duct with Mach number coincides precisely with the result given by eq. (22). This will provide confidence that the convective effects upon radiation are being properly modeled. Then the more interesting case of different Mach numbers within and outside the duct will be derived.

Resultant Axial Propagation Angle in the Duct

The geometry of the wave propagation vectors is shown in fig. 1, and the derivation which follows is considered to be done at the outer wall. Since the axial propagation angle Φ_x does not vary with radius in the present approximate analysis it is not crucial with regard to the radial position used. However in appendix A, the exact solution using Hankel functions show Φ_x to actually be a function of radius so the approximate analysis is truly valid only near the outer wall.

In fig. 1, the vector c (speed of sound) is normal to the wavefront. The propagation angles Φ_x, Φ_r, and Φ_θ are the angles between the vector c and the coordinate axes and are calculated as in eqs. (12), (19), and (20). The components of c are calculated from,

$$c_i = c \cos \Phi_i, \quad i = x, r, \theta \qquad (23)$$

The resultant direction of propagation will not be normal to the wave front but will be in the direction of the resultant vector c_R. The steady flow velocity ($c M_D$) must be added to c_x in a manner similar to that done in refs. 6 and 7. The resultant vector c_R contains the combined effect, due to duct Mach number, of the change in wave front directions and the drift velocity.

The angle which is now of interest for comparison with the far-field radiation principal lobe peak (eq. (22)) is the angle Ψ between the resultant vector c_R and the duct axis (x). This angle can be defined by,

$$\cos \Psi = \frac{c_x + cM_D}{c_R} \qquad (24)$$

The vectors c_R and c_θ are considered constant in the derivation. After some manipulation the numerator of eq. (24) can be shown to be,

$$c_x + cM_D = \frac{c(1 - M_D^2)\sqrt{1 - \frac{1}{\xi^2}}}{1 - M_D\sqrt{1 - \frac{1}{\xi^2}}} \qquad (25)$$

and c_R is,

$$c_R = \frac{c\sqrt{(1 - M_D^2)\left[1 + M_D\sqrt{1 - \frac{1}{\xi^2}}\right]}}{\sqrt{1 - M_D\sqrt{1 - \frac{1}{\xi^2}}}} \qquad (26)$$

Thus eq. (24) becomes

$$\cos \Psi = \sqrt{1 - M_D^2} \left\{ \frac{1 - \frac{1}{\xi^2}}{1 - M_D^2\left(1 - \frac{1}{\xi^2}\right)} \right\}^{1/2} \qquad (27)$$

A comparison of eqs. (22) and (27) shows that they are identical. The subscript appears on M_D in eq. (27) to denote that it is the Mach number in the duct. As the wave front leaves the duct, the angle Φ_x will not be changed (refraction effects neglected) and if the Mach number outside the duct is the same as in the duct (as assumed for derivation of eq. (22) in ref. 3) then the drift velocity effect is also the same as in the duct. Thus it is now evident that for the case which can be checked by exact radiation analysis that the resultant axial propagation angle in the duct is identical to the angle of the peak of the principal lobe in the far field.

Some other interesting observations can be made from the above relationships. The axial component of the resultant velocity vector c_R, as given by eq. (25), is the axial group velocity which could be derived from eq. (3) by applying

$$V_{gx} = \frac{d\omega}{dk_x} \qquad (28)$$

Also at mode cut-off ($\xi = 1$) the axial group velocity is zero and $\Psi = 90^\circ$. In contrast, from eq. (12), the axial propagation angle Φ_x at cut-off is,

$$\cos \Phi_x \Big|_{\xi=1} = -M_D \qquad (29)$$

As an example for an inlet with $M_D = -0.4$, $\Phi_x = 66.4^\circ$ while for an exhaust duct with $M_D = +0.4$, $\Phi_x = 113.6$. Thus, for an inlet, the wave front is tilted toward the axis which has important implications upon static test radiation patterns as will become more evident in the next section. For the exhaust case the wave appears to be going in the wrong direction at mode cut-off. It is the angle Ψ and not Φ_x which governs the sound propagation in the duct. This convective drift velocity effect has been used in refs. 6 and 7, however, it was not related to modal properties.

Effect of External Mach Number on Far-Field Radiation

Previous far field radiation theories applicable to engine inlets[3,12] have dealt with the special cases of zero Mach number or uniform Mach number inside and outside the duct. For an exhaust duct, differences in duct Mach number and external Mach number across a discontinuous slip layer have been handled in an exact analysis by Savkar[14] and in an approximate ray tracing approach by Jacques.[7] However, for an engine inlet there are no sharp discontinuities along cylindrical surfaces out in front of the inlet which would be required for these latter two studies to be valid. The following analysis is proposed to account for changes in the far-field radiation pattern occurring in static tests and in tests with external flow.

In the previous sections the effects of duct Mach number upon the angles of propagation in the duct have been derived and have been shown to be considerable. The propagation angle which has been shown to be controlling for the far-field radiation (when properly corrected for convective drift velocity) is that between the wave front normal and the duct axis. As the wave front passes out of the duct inlet, only diffraction and refraction can change the direction of this wave front. Diffraction scatters the sound and causes the lobed pattern in the far-field, but the bulk of the acoustic power still radiates in the predesignated direction determined by the resultant axial propagation angle. Refraction through velocity or temperature gradients can bend the wave fronts and could possibly be included prior to the application of the following analysis. For the present, however, refraction effects will be neglected.

It is thus assumed that the axial propagation angle ψ_x derived in the duct environment is also valid in the far-field. It is thus only necessary to apply the external drift velocity correction which in general will be different from that of the duct.

In the far-field, the normal to the wave front lies essentially in the radial-axial plane and only axial and radial velocity components need to be considered in a cylindrical coordinate system. Fig. 2 shows a sketch of the velocity vectors. All that needs to be done is to apply the external field (flight or static) drift velocity correction to the vector c. Recall that ψ_x is unchanged from its value in the duct and is given by,

$$\cos \psi_x = \frac{c_x}{c} = \frac{k_x}{k\left(1 - M_D \frac{k_x}{k}\right)} \tag{30}$$

The principal lobe of radiation can be expected at an angle where,

$$\cos \psi_p = \frac{c_x + cM_\infty}{c_R} \tag{31}$$

After some manipulations this angle can be expressed by,

$$\cos \psi_p = \left[M_\infty - M_D + (1 - M_D M_\infty)\sqrt{1 - \frac{1}{\xi^2}}\right] \Bigg/ \left\{\left[1 - M_D\sqrt{1 - \frac{1}{\xi^2}}\right]\left[1 + M_\infty(M_\infty - 2M_D) + (2M_\infty - M_D - M_D M^2)\sqrt{1 - \frac{1}{\xi^2}}\right]\right\}^{1/2} \tag{32}$$

If the external velocity is the same as the duct steady flow velocity, then eq. (32) reduces to the special case of eq. (27). Eq. (32) can be considered as an equation describing the effect of a wind tunnel velocity since in general $M_\infty \neq M_D$.

Far-Field Angles for Static Tests

An important special case of eq. (32) is that of $M_\infty = 0$ which is applicable for static engine tests. Eq. (32) then reduces to

$$\cos \psi_p\Big)_{M_\infty=0} = \frac{-M_D + \sqrt{1 - \frac{1}{\xi^2}}}{1 - M_D\sqrt{1 - \frac{1}{\xi^2}}} \tag{33}$$

which is of course the same as the ψ_x relationship given by eq. (12). Sample calculations using eq. (33) are shown in fig. 3. Of particular interest are the modes near cut-off. If the duct Mach number is zero, the principal lobe of far-field radiation will occur at 90°. This of course is also predicted by previous radiation theories when $M_D = 0$ or when $M_D = M_\infty$. However, as the inlet duct Mach number increases, the near cut-off modes propagate more toward the axis. For example at a typical inlet Mach number of -0.4, $\psi_p = 66.4°$. At $M_D = -0.8$, $\psi_p = 36.7°$ which must account for at least some of the apparent sideline attenuation of a near sonic inlet static test. For modes above cut-off the same trends are observed with a shift of the sound radiation toward the axis.

The results shown in fig. 3 are qualitatively corroborated by acoustic suppression results for the blade passage frequency as reported in refs. 15 and 16. The maximum suppression occurred at 70° (only 10° intervals measured) from the inlet at full engine speed with a Mach number $M_D = -0.375$. For these static tests the blade passage frequency should be rich in modal content near cut-off. Previous radiation theories would thus predict a peak attenuation near 90° for these most easily attenuated modes near cut-off. The present radiation theory, eq. (33) or fig. 3, would predict that peak attenuation should occur near 68° which is in good agreement with experimental results. Also apparent in the data of refs. 15 and 16, is the fact that as engine operating speed and the Mach number is reduced the peak attenuation moves more toward the sideline which is also in agreement with the present theory.

Far-Field Radiation with External Flow

Fig. 4 shows the far-field radiation peak for near cut-off modes when the surrounding medium is also moving which would simulate a wind tunnel test. Eq. (32) was used with $\xi = 1$ for various duct Mach

numbers (M_D) and external flow Mach number (M_∞). When $M_\infty = 0$ the results are the same as in fig. 3. However, as the tunnel speed increases (M_D presumed to remain nearly constant) the sound radiation moves back toward the sideline. For example, sample external velocities simulating approach and takeoff conditions are shown on fig. 4. For the approach condition ($M_D = -0.4$) a static test would show the near cutoff modes propagating at about 66° while in a wind tunnel this radiation would occur near 78° for $M_\infty = -0.2$. The difference between a take-off static and tunnel test would be 15° (from 53° to 68°).

Since there is a difference between static and wind tunnel far-field radiation patterns even for a specific mode, a correction should be applied to wind tunnel data before it is used in a fly-over calculation. Assuming that an inflow control device has been used in the static tests so that flight modal structure has been simulated, the difference between the static test angles (Φ_x) and the tunnel test angles (Ψ_p) must be reconciled. An expression can be derived relating these two angles by eliminating the cut-off ratio (ξ) between eqs. eqs. (12) and (32) or more simply by considering the geometric relations shown in fig. 2. The final expression is,

$$\cos \Psi_p = \frac{(M_\infty + \cos \Phi_x)}{\sqrt{1 + M_\infty^2 + 2M_\infty \cos \Phi_x}} \qquad (34)$$

This is equivalent to the expression of ref. 17 which deals with external convective effects upon noise radiation. This expression shows that those modes which propagate at far-field angle Φ_x in a static test, will propagate at angle Ψ_p in a wind tunnel test. This correction can be considerable. For example, with a tunnel speed of only $M_\infty = -0.2$, the static data measured at 50°, 60°, and 70° should be shifted to 60°, 71°, and 81.5° for a wind tunnel test. This will have the effect of shifting the usually higher sound pressure level data of these forward angles back more toward the sideline. It was assumed in the above discussion that the principal lobes dominate the radiation pattern and that even for a multimodal pattern the shift will thus be properly described by eq. (34).

Technically a correction should also be made for the sound pressure level when the angle shift of eq. (34) is made. By maintaining acoustic power and accounting for the principal lobe width change (solid angle change) which occurs with the angle shift the following expression can be derived,

$$\frac{P_\infty^2}{P_o^2} \approx \frac{(1 + M_\infty^2 + 2M_\infty \cos \Phi_x)^{3/2}}{(1 + M_\infty \cos \Phi_x)} \qquad (35)$$

For tunnel Mach numbers between -0.2 and -0.4 the sound pressure level shift for the static test angles between 50° and 90° is less than 1.5 dB. Thus for the sideline angles of most interest the sound pressure level correction is probably not significant, although the angle shift of eq. (34) should definitely be considered. It should again be noted that refraction effects within the velocity gradients near the inlet for static tests have not been considered here. These effects should not be great, however, for the near sideline angles of most interest.

While the radiation theory presented in this paper appears to receive preliminary confirmation from static engine tests, there is not yet any confirmation of the wind tunnel effects since there were no data available. Careful testing would be required to insure that the results were not masked by other factors. For example, the modal structure of a fan source would be expected to be different for static testing than for wind tunnel testing.[18] Inflow control devices (screens) would be required to provide a static test noise source which would have a chance to simulate the modal content produced by a turbofan in a wind tunnel.

It should be noted that the corrections discussed above must be made for data obtained in a wind tunnel test since it is the directivity pattern described as a function of Φ_x and not Ψ_p which is projected to the stationary observer in a simulated fly-over calculation.

Concluding Remarks

The angles of propagation for the wave front making up a duct mode have been presented here with Mach number in the duct. Approximate equations have been derived to provide simple utilitarian expressions. These expressions are valid only near the outer wall which is the most important region since the bulk of the acoustic intensity is located there and this is also where incidence angles would be of interest. Exact solutions using Hankel functions are given in appendix A and these corroborate the approximate solution accuracy near the outer wall. The main emphasis of this paper was to use the axial propagation angle to infer information about the far-field radiation pattern. The resultant axial angle of propagation in the duct was shown to agree exactly with the peak of the principal lobe of far-field radiation obtained from formal radiation calculations when the Mach number is uniform everywhere. The present solution was then extended to cover the case of different Mach numbers inside and outside the duct for which exact calculations have not been available for engine inlet configurations. The new analysis shows that for static engine tests the inlet radiation can be expected to be shifted considerably toward the inlet axis over that obtained from previous analysis. This static test radiation shift can be shown to have preliminary verification. An external Mach number convective effect is also predicted which would shift the sound radiation back toward the sideline (compared to a static test) as the external flow velocity increases. The refraction of the sound by the flow gradients near the inlet could possibly be included in the analysis, but this effect has not been included here.

Appendix A

Cylindrical Wave Synthesis of a Ducted Spinning Mode

The exterior radiation field of an infinite cylinder sustaining standing circumferential surface oscillations, synchronous in the axial direction, is shown by Morse and Ingard[19] to be described by the Hankel function combination, $\cos(m\theta)\, H_m^{(1)}(kr)\, \exp(-i\omega t)$. As a separate matter in the same reference it is demonstrated that the modal components of the pressure field inside a hardwall rectangular duct may be synthesized by complementary pairs of inward and outward plane wave trains.

These concepts may be combined and extended to describe the field of a spinning mode in a cylindrical duct.

Let the (complex) pressure $P_m = P_m(x,\theta,r,t)$ in the duct be expressed as the sum of a pair of cylindrical waves:

$$P_m = P_m^1 + P_m^2 \tag{A-1}$$

The radially outward wave is given by

$$P_m^1 = \frac{1}{2} C_{m\mu} H_m^{(1)}\left(\frac{\alpha r}{r_o}\right) e^{i(k_x x+m\theta-\omega t)} \tag{A-2}$$

and the matching inward wave is

$$P_m^2 = \frac{1}{2} C_{m\mu} H_m^{(2)}\left(\frac{\alpha r}{r_o}\right) e^{i(k_x x+m\theta-\omega t)} \tag{A-3}$$

The eigenvalue α as in the main text should contain the subscripts m,μ but these have been dropped for brevity. $H_m^{(1)}$ and $H_m^{(2)}$ are Hankel functions of the first and second kinds:

$$H_m^{(1)} = J_m + i\,Y_m$$
$$H_m^{(2)} = J_m + i\,Y_m \tag{A-4}$$

Inward and outward wave designations are applied as a consequence of the far-field nature of P_m^1 and P_m^2 which is disclosed by the asymptotic behavior of the Bessel functions:

$$P_m^1, P_m^2 \underset{\frac{\alpha r}{r_o}\to\infty}{\rightarrow} \frac{1}{2} C_{m\mu} \sqrt{\frac{2r_o}{\pi\alpha r}}\, e^{i\left[k_x x+m\theta\pm\frac{\alpha r}{r_o}-\omega t\mp\frac{(2m+1)}{4}\pi\right]} \tag{A-5}$$

Two comments may be helpful. First, it is obvious from eqs. (A-2), (A-3), that the sum of P_m^1 and P_m^2 gives the duct mode field of eq. (2). Second, the opposite signs applicable to P_m^2 require the wave to move radially inward in order to conserve phase.

The near-field behavior of the outward wave may be found by representing the Hankel function $H_m^{(1)}$ in polar form:

$$H_m^{(1)}\left(\frac{\alpha r}{r_o}\right) = h_m\left(\frac{\alpha r}{r_o}\right) e^{i\Phi_m\left(\frac{\alpha r}{r_o}\right)} \tag{A-6}$$

where the amplitude

$$h_m\left(\frac{\alpha r}{r_o}\right) = \left[J_m^2\left(\frac{\alpha r}{r_o}\right) + Y_m^2\left(\frac{\alpha r}{r_o}\right)\right]^{1/2} \tag{A-7}$$

and Φ_m, the phase of H_m^1, is

$$\Phi_m\left(\frac{\alpha r}{r_o}\right) = \arctan\left[\frac{Y_m\left(\frac{\alpha r}{r_o}\right)}{J_m\left(\frac{\alpha r}{r_o}\right)}\right] \tag{A-8}$$

With these substitutions, the general outward wave expression, eq. (A-2) becomes

$$P_m^1 = \frac{1}{2} C_{m\mu}\, h_m\left(\frac{\alpha r}{r_o}\right) e^{i\left[k_x x+m\theta+\Phi_m\left(\frac{\alpha r}{r_o}\right)-\omega t\right]} \tag{A-9}$$

The local wave direction and phase velocity are obtained by examining the exponent

$$\chi = k_x x + m\theta + \Phi_m\left(\frac{\alpha r}{r_o}\right) - \omega t \tag{A-10}$$

A plane that is locally tangent to the wave front will be governed by the requirement that the phase, χ is conserved over a small displacement occurring during a corresponding small time interval. For this phase conservation $d\chi = 0$ or

$$d\chi = k_x dx + m d\theta + \frac{d}{dr}\Phi_m\left(\frac{\alpha r}{r_o}\right) dr - \omega dt = 0 \tag{A-11}$$

Writing

$$\Phi_m'\left(\frac{\alpha r}{r_o}\right) = \frac{d}{d\left(\frac{\alpha r}{r_o}\right)}\Phi_m\left(\frac{\alpha r}{r_o}\right) \tag{A-12}$$

and introducing the circumferential arc length coordinate

$$s = r\theta \tag{A-13}$$

the equation of the local phase plane becomes

$$k_x dx + \frac{m}{r} ds + \frac{\alpha}{r_o}\Phi_m'\left(\frac{\alpha r}{r_o}\right) dr = \omega dt \tag{A-14}$$

or

$$k_x dx + k_s ds + k_r dr = \omega dt \tag{A-14a}$$

The coefficients of the differential coordinates in (A-14) are the axial, tangential, and radial components of the local wave number vector, denoted by $\vec{K}$. On dividing (A-14) by the magnitude of $\vec{K}$, denoted by K there follows:

$$\cos\Psi_x\, dx + \cos\Psi_s\, ds + \cos\Psi_r\, dr = \frac{\omega}{K} dt \tag{A-15}$$

where

$$\left.\begin{aligned} \cos\Psi_x &= k_x/K \\ \cos\Psi_s &= \cos\Psi_\theta = \frac{m}{r}\Big/K \\ \cos\Psi_r &= \frac{\alpha}{r_o}\Phi_m'\left(\frac{\alpha r}{r_o}\right)\Big/K \end{aligned}\right\} \tag{A-16}$$

$$K = \left\{k_x^2 + \left(\frac{m}{r}\right)^2 + \left[\frac{\alpha}{r_o}\Phi_m'\left(\frac{\alpha r}{r_o}\right)\right]^2\right\}^{1/2} \tag{A-17}$$

Eq. (A-15) is the normal form of a plane with direction angles Ψ_x, Ψ_s, Ψ_r, traveling at a local phase velocity $V_{ph} = \omega/K$. If K is expressed as:

$$K = kK' = k\left\{\left(\frac{k_x}{k}\right)^2 + \left(\frac{m}{k_r}\right)^2 + \left[\frac{\alpha}{r_o k}\,\Phi'_m\left(\frac{\alpha r}{r_o}\right)\right]^2\right\}^{1/2} \qquad \text{(A-18)}$$

the magnitude of the phase velocity becomes

$$V_{ph} = \frac{\omega}{K} = \frac{\omega}{kK'} = \frac{c}{K'} \qquad \text{(A-19)}$$

Thus the phase velocity differs from the speed of sound by the factor $1/K'$. It can be shown that $K' > 1$ and approaches 1 as $(\alpha r/r_o) \to \infty$, so that the near-field phase velocity is always subsonic. This means that the sum of the squares of the wave numbers k_x, k_s, k_r, add up to K^2, which is larger than the square of the ordinary wave number, $k = \omega/c$.

Further work requires evaluation of $\Phi'_m(\alpha r/r_o)$, the derivative of the phase of the Hankel function $H_m^{(1)}(\alpha r/r_o)$. It is found that

$$\Phi'_m\left(\frac{\alpha r}{r_o}\right) = \frac{2\,r_o}{\pi \alpha r\left[J_m^2\left(\frac{\alpha r}{r_o}\right) + Y_m^2\left(\frac{\alpha r}{r_o}\right)\right]} \qquad \text{(A-20)}$$

This expression allows computation of the local wave speed and direction angles for a wave at any radius using eqs. (A-16) to (A-19).

Some calculations were made for the wall radius location $r = r_o$, in the $M_D = 0$ case, for cutoff ratios of 1 and 2. The tabulation in table A1 presents values of K' and the wall incidence angle Ψ_r (eq. (A-16)). For comparison, values of Ψ_r computed from the main text eq. (21), which is based on the approximation $K = k$ or $K' = 1$, are included. These values show that the greatest departures from "conventional" or far-field behavior occur near cutoff for the lowest order m and μ modes. The departures, however, are quite minor: For the "worst" case, the (1,0) mode at cutoff, the phase velocity departs from sonic by only 6 percent and the exact and approximate wall incidence angles differ by about 2°. Thus the essential assumption used in deriving the results of the main text, namely that for $M_D = 0$ the squares of the axial, tangential, and radial wave-number components sum to the square of the ordinary wave number, $k = \omega/c$, at the wall radius, is in excellent practical agreement with results of the exact analysis. This assumption implies that the eigenvalues, which are independent of M_D, are related by $k_s^2 + k_{r_o}^2 = k_{r\theta}^2 = (\alpha/r_o)^2$.

Finally, it may be of some interest to note that the situation changes radically as the duct axis is approached more closely. Calculations show the following ($m \neq 0$):

$$K' \to \infty$$

$$V_{ph} \to 0$$

$$\Psi_x \to 90^\circ$$

$$\Psi_s \to 0$$

$$\Psi_r \to 90^\circ$$

Thus near the axis the local wave velocity is very small and is essentially circumferential in direction. This contrasts with the wall behavior where the phase velocity is almost sonic and the wave direction is predominantly axial-radial.

TABLE A1. - VALUES OF K' AND Ψ_r FOR $M_D = 0$, $r = r_o$

Mode (m,μ)	Cutoff ratio ξ = 1			Cutoff ratio ξ = 2		
	K'	Ψ_r(exact)	Ψ_r(approx)	K'	Ψ_r(exact)	Ψ_r(approx)
		deg			deg	
1,0	1.0633	30.7	32.9	1.0162	63.3	65.2
1,1	1.0050	10.8	10.8	1.0013	60.5	60.6
1,2	1.0018	6.7	6.7	1.0005	60.2	60.2
2,0	1.0462	38.8	40.9	1.0117	66.2	67.8
2,1	1.0043	17.3	17.4	1.0011	61.4	61.5
2,2	1.0019	11.6	11.6	1.0005	60.6	60.7
4,0	1.0334	46.7	48.8	1.0084	69.4	70.8
4,1	1.0030	25.4	25.8	1.0008	63.1	63.2
4,2	1.0012	18.4	18.4	1.0003	61.6	61.7
8,0	1.0232	54.1	56.0	1.0059	72.7	73.8
8,1	1.0030	34.4	34.5	1.0002	65.6	65.7
8,2	1.0010	26.7	26.7	1.0002	63.5	63.5
16,0	1.0158	60.7	62.4	1.0040	75.7	76.6
16,0	1.0018	43.4	43.5	1.0004	68.7	68.7
16,2	1.0010	35.8	35.8	1.0002	66.1	66.1

Appendix B

Wave-front Propagation Angles with Flow

This appendix is intended to provide a simplified example of obtaining the angles of propagation of the wave fronts in a duct with flow. To serve this purpose a simple two dimensional rectangular geometry will be used. The wave equation solution can be given as,

$$p = e^{i(\omega t - k_x X)} \cos k_y Y$$

$$= \frac{1}{2} e^{i(\omega t - k_x X)} \left[e^{-ik_y Y} + e^{+ik_y Y} \right] \qquad \text{(B-1)}$$

The second representation in eq. (B-1) breaks the modal cosine function into the two wave fronts representing this mode. The first wave travels in the +y direction while the second wave travels in the -y direction. Concentrating on the +y, moving wave the exponential phase quantities are gathered together and set equal to a constant to represent a constant phase line or wave front as,

$$\omega t - k_x x - k_y y = \text{constant} \qquad \text{(B-2)}$$

If time t is also considered as a constant, an instantaneous representation of the slope of the wave front can be obtained by differentiating eq. (B-2) to obtain,

$$\frac{dy}{dx} = -\frac{k_x}{k_y} \qquad \text{(B-3)}$$

Now a sketch of the wave front can be constructed as in fig. B1. The angles of interest are ζ_x and ζ_y the angles between the wave front normal and the coordinate axes. By similarity of triangles these angles can also be identified in the triangle drawn to show the wave front slope. It is now obvious that,

$$\cos \zeta_x = \frac{k_x}{\sqrt{k_x^2 + k_y^2}} = \frac{k_x}{\sqrt{\sum_i k_i^2}} \qquad \text{(B-4)}$$

and

$$\cos \zeta_y = \frac{k_y}{\sqrt{k_x^2 + k_y^2}} = \frac{k_y}{\sqrt{\sum_i k_i^2}} \qquad \text{(B-5)}$$

Up to this point in the derivation there was no consideration of the duct Mach number M_D. This effect is obtained by inserting the pressure solution into the wave equation to obtain the relationship between the wave numbers as,

$$k_x^2 + k_y^2 = k^2 - 2 M_D k k_x + M_D^2 k_x^2 = (k - M_D k_x)^2 \qquad \text{(B-6)}$$

which is similar to eq. (3) in the main text. Eq. (B-6) immediately gives

$$\sqrt{k_x^2 + k_y^2} = k - M_D k_x \qquad \text{(B-7)}$$

and some rearrangement of eq. (B-6) yields,

$$k_x = \frac{k\left[-M_D + \sqrt{1 - (1 - M_D^2)\left(\frac{k_y}{k}\right)^2}\right]}{1 - M_D^2} \qquad \text{(B-8)}$$

The wave number k_y is not a function of M_D, but since the denominators of eqs. (B-4) and (B-5) are functions of M_D, then both φ_x and φ_y depend upon duct Mach number.

References

1. Wright, S. E., "Waveguides and Rotating Sources," Journal of Sound and Vibration, Vol. 25, Nov. 1972, pp. 163-178.
2. Candel, S. M., "Acoustic Radiation from the End of a Two-Dimensional Duct - Effects of Uniform Flow and Duct Lining," Journal of Sound and Vibration, Vol. 28, May 1973, pp. 1-13.
3. Homicz, G. F. and Lordi, J. A., "A Note on the Radiative Directivity Patterns of Duct Acoustic Modes," Journal of Sound and Vibration, Vol. 41, Aug. 1975, pp. 283-290.
4. Rice, E. J., "Acoustic Liner Optimum Impedance for Spinning Modes with Mode Cut-off Ratio as the Design Criterion," AIAA Paper 76-516, July 1976.
5. Rice, E. J., "Inlet Noise Suppressor Design Method Based Upon the Distribution of Acoustic Power with Mode Cut-off Ratio," Advances in Engineering Science, NASA CP-2001, Vol. 3, 1976, pp. 883-894.
6. Posey, J. W., "High Frequency Sound Attenuation in Short Flow Ducts," NASA TM-78708, 1978.
7. Jacques, J. R., "Aircraft Flight Effects on High Frequency Sound Emerging from a Constant Area Jet Pipe Flow," Journal of Sound and Vibration, Vol. 45, Apr. 1976, pp. 569-582.
8. Rice, E. J., "Modal Propagation Angles in Ducts with Soft Walls and Their Connection with Suppressor Performance," proposed paper for the 5th AIAA Aeroacoustic Conference, Seattle, Wash., March 12-14, 1979.
9. Sofrin, T. G. and McCann, J. F., "Pratt and Whitney Experience in Compressor-Noise Reduction," abstracted in Journal of the Acoustical Society of America, Vol. 40, 1966, pp. 1248-1249. (Also presented (paper 2D2) at 72nd Meeting of the Acoustical Society of America, Los Angeles, California, Nov. 1966.)
10. Rice, E. J., "Multimodal Far-Field Acoustic Radiation Pattern using Mode Cutoff Ratio," AIAA Journal, Vol. 16, Sept. 1978, pp. 906-911. Also NASA TM-73721.
11. Cumpsty, N. A., "Tone Noise from Rotor/Stator Interactions in High Speed Fans," Journal of Sound and Vibration, Vol. 24, Oct. 1972, pp. 393-409.
12. Lansing, D. L., Drischler, J. A., and Pusey, C. G., "Radiation of Sound From An Unflanged Circular Duct with Flow," paper presented at the 79th Meeting of the Acoustical Society, Atlantic City, N. J., April 21-24, 1970.
13. Saule, A. V. and Rice, E. J., "Far-Field Multimodal Acoustic Radiation Directivity," NASA TM-73839, 1977.

14. Savkar, S. D.,"Radiation of Cylindrical Duct Acoustic Modes with Flow Mismatch," Journal of Sound and Vibration, Vol. 42, Oct. 1975, pp. 363-386.

15. Heidelberg, L. J., Rice, E. J., and Homyak, L., "Experimental Evaluation of a Spinning Mode Acoustic Treatment Design Concept for Aircraft Inlets,"Proposed NASA Technical Paper.

16. Heidelberg, L. J. and Homyak, L., "Full-Scale Engine Tests of Bulk Absorber Acoustic Inlet Treatment," proposed paper for presentation at the AIAA 5th Aeroacoustics Conference, Seattle, Washington, March 12-14, 1979.

17. Williams, John, "Ground-Based Facilities with Forward-Speed Representation for Aircraft Noise Research," Aerodynamic Noise, AGARD-LS-80, 1977, pp. 11-1 to 11-43.

18. Heidmann, M. F. and Dietrich, D. A., "Simulation of Flight-Type Engine Fan Noise in the NASA-Lewis 9x15 Anechoic Wind Tunnel," NASA TM X-73540, 1976.

19. Morse, P. M. and Ingard, K. U., Theoretical Acoustics, McGraw-Hill, New York, 1968.

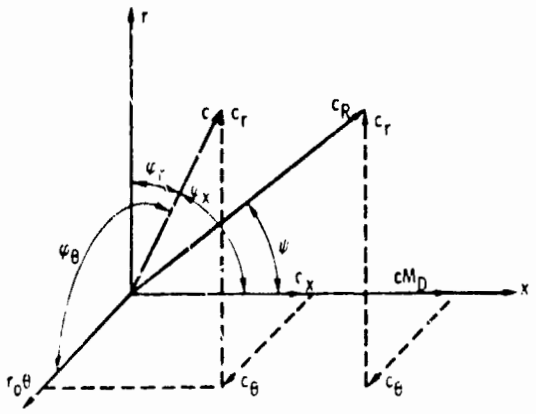

Figure 1. - Sketch of the propagation angles in the duct.

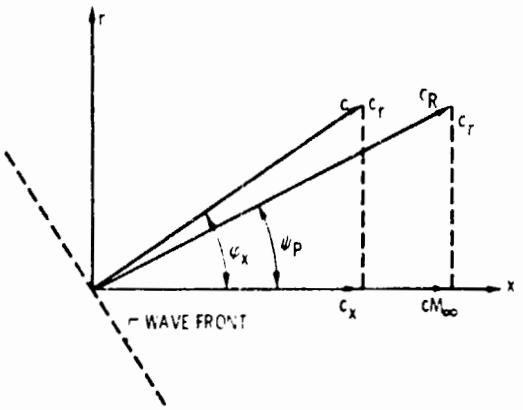

Figure 2. - Far-field propagation angles with flow.

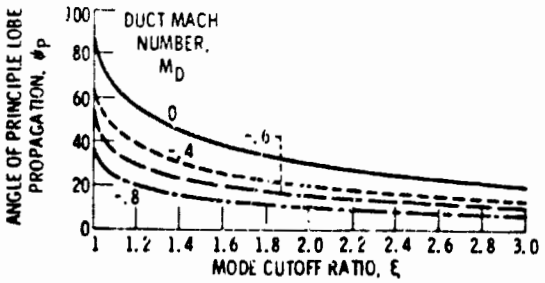

Figure 3. - Convective effect upon far-field radiation principle lobe angle for inlets under static test, $M_\infty = 0$.

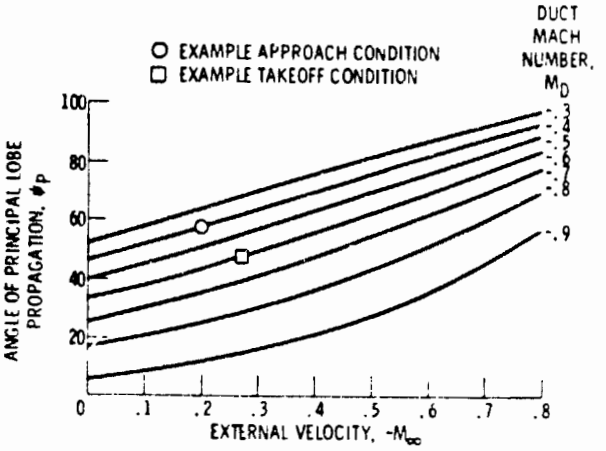

Figure 4. - Effect of external and duct velocities on far-field propagation angle for near cutoff modes.

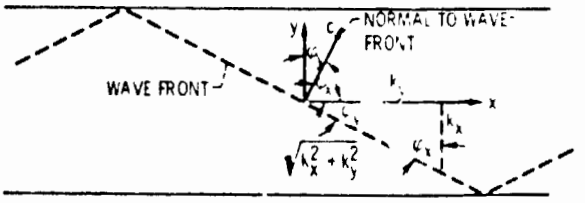

Figure B1. - Sketch of propagation angles and wavefront slope in a two dimension rectangular duct.